RSC Advances

PAPER

View Article Online
View Journal | View Issue

Cite this: *RSC Adv.*, 2015, **5**, 10632

A simple route to $CoFe_2O_4$ nanoparticles with shape and size control and their tunable peroxidase-like activity†

Ke Zhang, Wei Zuo, Zhiyi Wang, Jian Liu, Tianrong Li, Baodui Wang* and Zhengyin Yang*

Recent studies have suggested that the physical and chemical properties of nanoparticles (NPs) strongly depend on local chemical composition, size, and shape. Here, we report a new precursor-mediated growth of monodisperse magnetic cobalt ferrite ($CoFe_2O_4$) NPs with controlled size and shape. $CoFe_2O_4$ NPs with near corner-grown cubic, near cubic and polyhedron shape can be successfully prepared by simply tuning the amount of iron and cobalt acetylacetonates in oleic acid. Interestingly, the product shape varies from near corner-grown cubic to starlike by only changing the reaction temperature from 320 °C to 330 °C. These $CoFe_2O_4$ NPs exhibit size and shape-dependent peroxidase-like activity towards 3,3′,5,5′-tetramethylbenzdine (TMB) in the presence of H_2O_2, and thus exhibited different levels of peroxidase-like activities, in the order of spherical > near corner-grown cubic > starlike > near cubic > polyhedron; this order was closely related to their particle size and crystal morphology. $CoFe_2O_4$NPs exhibited high stability in HAc–NaAc buffer (pH = 4.0) and high activity over a broad pH (2.5–6.0). Furthermore, the Michaelis constants K_m value for the $CoFe_2O_4$ NPs (0.006 mM) with TMB as the substrate was lower than HRP (0.062 mM) and Fe_3O_4 NPs (0.010 mM). After further surface functionalization with folic acid (FA), the folate-conjugated $CoFe_2O_4$ nanoparticles allow discrimination of HeLa cells (folate receptor overexpression) from NIH-3T3 cells (without folate receptor expression). Such investigation is of great significance for peroxidase nanomimetics with enhanced activity and utilization.

Received 20th December 2014
Accepted 5th January 2015

DOI: 10.1039/c4ra15675g

www.rsc.org/advances

1. Introduction

The ability to synthesize monodisperse magnetic nanoparticles (MNPs) with desired sizes and shapes is of great importance in exploring their applications in catalysis, sensors, microelectronics, and many other areas of nanotechnology.[1] $CoFe_2O_4$ ferrite (CF), which is a well-known inverse spinel with Co^{2+} ions on B sites and Fe^{3+} ions distributed equally among A and B sites,[2] has attracted considerable attention for its potential applications such as in catalysis, as an anode material for lithium ion batteries, in biomedicine, and as enzymatic mimetics.[3–6] The properties can be additionally tuned by controlling the shape, size, and crystallinity of the nanocrystals. Various synthetic strategies have been devoted to preparing $CoFe_2O_4$ nanoparticles with controlled size and shape. A range of methods, including coprecipitation, sol–gel methods, thermal decomposition, combustion reaction, and hydrothermal synthesis.[7–11] Among chemical methods, thermal decomposition of mixed organic Co^{2+} and Fe^{3+} compounds, such as metal acetylacetonates, metal carbonyls, *etc.*, in high boiling point solvents has proven to be an ideal approach for preparing monodisperse $CoFe_2O_4$ nanocrystals with high yield, narrow size distribution, and good crystallinity.[12] As we well known, the shape and size of the NPs using this method were controlled by adjusting the surfactant to precursor ratio, heating rate, stirring, and seed mediated growth during the reaction.[13] Despite this progress, these control methods require precise process management of environmental conditions or necessitate tedious multistep reaction that are not necessarily amenable to large scale NP synthesis. Thus, exploring facile and effective synthesis method is still a challenging task for the controlled synthesis of $CoFe_2O_4$ NPs with desirable size, shape, and composition.

Exploitation of new functions of known nanomaterials is one of the most attractive aspects in nanoscience. Since magnetite nanoparticles were serendipitously discovered to have intrinsic peroxidase-like activity, they have been persued as peroxidase nanomimetics to catalyze and detect some molecules.[14] In addition, $CoFe_2O_4$ NPs have been found to possess intrinsic

Key Laboratory of Nonferrous Metal Chemistry and Resources Utilization of Gansu Province and State Key Laboratory of Applied Organic Chemistry, Lanzhou University Gansu, Lanzhou, 730000, P. R. China. E-mail: wangbd@lzu.edu.cn; yangzy@lzu.edu.cn; Fax: +86-931-8912582

† Electronic supplementary information (ESI) available. See DOI: 10.1039/c4ra15675g

oxidase-like activity.[15] However, to date, very little has been explored on the effect of the shape and size on the catalytic properties of peroxidase nanomimetics of cobalt ferrite nanostructures and little is known about the effects of different $CoFe_2O_4$ nanostructures on biocatalysis.

In this study, we demonstrate for the first time a general one-step synthesis of $CoFe_2O_4$ NPs *via* the co-thermolysis of iron and cobalt acetylacetonates precursors in the solvent of oleic acid. The different shape (polyhedrons, near corner-grown cubic, near cubic and starlike) and different size (15, 25, 45 and 35 nm) could be readily tuned by only change the decomposition amount of Co and Fe precursors. Additional experiments have surprisingly revealed that enhancement the reaction temperature at 330 °C can induce growth starlike $CoFe_2O_4$ NPs. Furthermore, we investigated the influence of various physical parameters like shape, size and surface area on the enzyme mimic properties of $CoFe_2O_4$ NPs. Kinetic parameters (V_{max} and K_m) of all the nanoparticles were assessed, and a correlative investigation between the various physical features of $CoFe_2O_4$ and its enzyme mimicking property is presented. On the basis of these findings, we have designed the folate-conjugated $CoFe_2O_4$ nanoparticles as a nanoprobe to provide dual functionality by binding to folate-expressing cancer cells and facilitating detection by catalytic oxidation of sensitive colorimetric substrates (dyes).

2. Experimental

2.1. Chemicals and instrumentation

$Fe(acac)_3$ (99.9%), $Co(acac)_2$ (99%), oleic acid (OA, technical grade, 90%), 1,2-hexadecanediol (HDD, technical grade, 90%), phenyl ether, and polyethylene glycol (MW = 4000) were purchased from Sigma Aldrich. Folic acid, dicyclohexylcarbodiimide (DCC), *N*-hydroxysuccinimide (NHS), 3,3′,5,5′-tetramethylbenzidine (TMB), *o*-phenylenediamine (OPD), 3,4-dihydroxybenzaldehyde and terephthalic acid were from Aladdin in China. Hydrogen peroxide (H_2O_2, 30%), sodium acetate anhydrous (NaAc, A.R.) and acetic acid (HAc, A.R.) were obtained from Beijing Chemicals Inc (Beijing, China). All chemicals were used without further purification, except DMF, $CHCl_3$, were used as anhydrous. Aqueous solutions were prepared with double-distilled water (dd-H_2O) from a Millipore system (>18 MΩ cm). 1, ω-diaminopolyoxyethylene (MW = 4000), PEG-3,4-dihydroxybenzylamine (DIB-PEG-NH_2) were synthesized according to the published method.[16] All the dialysis bags (MWCO 8000-14000) were obtained from Shanghai Med.

The TEM measurements were carried out with Philips EM 420 (120 kV) under ambient conditions deposition of the hexane or H_2O dispersions of the particles on amorphous carbon coated copper grids. The hysteresis loop was obtained at 300 K with a LakeShore 7400 VSM system. The fluorescence spectra were recorded on a Shimadzu RF-5301 spectrofluorophotometer. UV-vis absorbance measurements experiments were carried out on a UV 1750 spectrophotometer (Shimadzu, Japan). The absorbance was acquired on a 721E visible spectrophotometer (Shanghai). The cytotoxicity assay was detected by a microplate reader (Nanjing Huadong Electronics Group Co., Ltd. DG5033A – microplate reader).

2.2. Synthesis of $CoFe_2O_4$ nanoparticles

For synthesis of 15 nm $CoFe_2O_4$ nanoparticles, $Fe(acac)_3$ (8 mmol), $Co(acac)_2$ (4 mmol) and oleic acid (15 mL) were mixed and magnetically stirred under a flow of nitrogen. The mixture was heated to 120 °C under nitrogen atmosphere with vigorous stirring, and then kept at that temperature for 1 h. The obtained solution was then heated to 320 °C, and the solution color gradually became black, indicating that the magnetic nanoparticles were being formed. After refluxing for 4 h, the solution was cooled to room temperature, and a black precipitate was obtained upon addition of 50 mL of isopropyl alcohol and centrifuged. The product was washed with petroleum and ethanol (1/4, v/v) 3 times. Finally, the product was redispersed in hexane.

Under similar reaction conditions, the different size and shape $CoFe_2O_4$ NPs could be produced by simply controlling the amount of $Fe(acac)_3$ and $Co(acac)_2$. For example, the near corner-grown cubic NPs with 25 nm was synthesized using 2 mmol of $Fe(acac)_3$ and 1 mmol of $Co(acac)_2$, and the near cubic NPs with 45 nm was prepared using 4 mmol of $Fe(acac)_3$ and 2 mmol of $Co(acac)_2$. The amount of $Fe(acac)_3$ and $Co(acac)_2$ that synthesized star-shaped nanoparticles with 35 nm was same with the amount of that near corner-grown cubic NPs expect using 330 °C.

4 nm spherical $CoFe_2O_4$ NPs are prepared according to literature.[17] $Fe(acac)_3$ (2 mmol), $Co(acac)_2$ (1 mmol), 1,2-hexadecanediol (10 mmol), oleic acid (6 mmol), and phenyl ether (20 mL) were mixed and magnetically stirred under a flow of nitrogen. The mixture was heated to 200 °C and kept at this temperature for 30 min, and then, under a blanket of nitrogen, the mixture was heated to reflux (265 °C) and kept at this temperature for another 30 min. The dark red-brown mixture was cooled to room temperature by moving the heat source. Under ambient conditions, ethanol (40 mL) was added to the mixture, and a dark red-brown material was precipitated and separated *via* centrifugation (6000 rpm, 3 min). The dark red-brown product was dissolved in hexane (Fig. S1†).

2.3. Synthesis of $CoFe_2O_4$-DIB-PEG-NH_2 (1a) and $CoFe_2O_4$-DIB-PEG-NH_2-FA (1b)

DIB-PEG-NH_2 (100 mg) was dissolved in $CHCl_3$ (10 mL), and then the $CoFe_2O_4$ nanoparticles (10 mg) was added. The mixture was stirred 24 h at room temperature. The modified $CoFe_2O_4$ nanoparticles (water-soluble nanoparticles, abbreviated as **1a**) were precipitated by adding petroleum ether, and collected by centrifugation at 4500 rpm (3 min). The product was washed with ethanol and petroleum (1/4, v/v) 3 times. Finally, the product was redispersed in double-distilled water.

Folic acid (0.044 g, 0.1 mmol) was dissolved in 3 mL of dry dimethyl sulphoxide (DMSO) into which 0.040 g (0.15 mmol) of dicyclohexylcarbodiimide (DCC) and 0.014 g (0.12 mmol) of hydroxysuccinimide (NHS) were added. The reaction mixture was stirred for 12 hours at room temperature and then added

with DIB-PEG-NH_2 (200 mg). After another 12 hours of reaction, the product was precipitated by adding diethyl ether (20 mL) and dried *in vacuo*. ^{1}HNMR of DIB-PEG-NH_2-FA (DMSO, 400 MHz): $\delta = 8.64$ (1H, s, C8), 7.65 (2H, d, $J = 8.4$ Hz, C13 and C15), 7.22 (1H, m, C26), 6.99 (1H, d, $J = 1.6$ Hz, C24), 6.75 (1H, m, C25), 6.63 (2H, d, $J = 8.4$ Hz, C12 and C16), 4.48 (2H, d, $J = 6.0$ Hz, C9), 4.32 (1H, m, C18), 3.64 (2H, dd, $J = 6.0$, 4.4 Hz, C21), 3.51 (~345H, bs, PEG3800), 3.19 (2H, td, $J = 11.0$, 5.4 Hz, C22), 2.54 (1H, s, C23), 2.25 (2H, m, C20), 1.93 ppm (2H, m, C19). The $CoFe_2O_4$-DIB-PEG-NH_2-FA (**1b**) was synthesized by DIB-PEG-NH_2-FA and the $CoFe_2O_4$ nanoparticles with the similar reaction conditions mentioned above.

2.4. Leaching of iron ions from $CoFe_2O_4$ and Fe_3O_4 NPs

To investigate the leaching of iron ions from the water-soluble $CoFe_2O_4$ and Fe_3O_4 NPs in the presence of HAc–NaAc buffer (pH = 4.0), they were put into dialysis bags and incubated them in the HAc–NaAc buffer. After incubating for 60 min, the leaching solution from the dialysis bags was added into H_2O_2–TMB system and their catalytic activities were tested. The same concentration iron of NPs as control was also measured.

2.5. Mechanism of peroxidase-like activity of 1a

10 μL of 0.4 mM terephthalic acid solution dissolved in DMF was added into 2 mL the HAc–NaAc buffer containing 500 μL of 10 mM H_2O_2 and different concentration of **1a** (0 μg and 30 μg).[18] Then the mixture solution was incubated at 37 °C for 10 h. After that, the reaction solution was detected by the fluorescence spectra under the 315 nm excitation. Under the same condition, the reaction solution without H_2O_2 was also measured.

2.6. The catalytic oxidation of TMB by 1a and steady-state kinetic assays

To investigate the peroxidase-like activity of the **1a**, the catalytic oxidation of TMB in the presence of H_2O_2 was tested. 500 μL of 100 mM H_2O_2 and 20 μL of 15 mM TMB (prepared freshly) were added to 2 mL of HAc–NaAc buffer (pH = 4.0). Then, a certain amount of **1a** suspension was added into the above mixture. The oxidation reaction progress was monitored at 37 °C with 2 min intervals by recording the absorption spectra in a scanning kinetics mode. Steady-state kinetic assays were carried out at 37 °C in 0.2 M HAc–NaAc buffer (pH = 4.0) in the presence of **1a**. For TMB as a substrate, the H_2O_2 concentration was fixed at 100 mM. For H_2O_2 as a substrate, the TMB concentration was fixed at 15 mM. All the reactions were monitored at 653 nm using a 721E visible spectrophotometer. The apparent kinetic parameters were calculated based on the function $v = V_{max} \times [S]/(K_m + [S])$, where v is the reaction velocity, V_{max} is the maximal reaction velocity, [S] is the concentration of substrate and K_m is the Michaelis constant.

2.7. Cytotoxicity and bioassay assay

The cytotoxicity of the **1b** *in vitro* was evaluated by performing methyl thiazolyl tetrazolium (MTT) assay of the HeLa cells incubated with the different nanoparticles. Cells were seeded into a 96-well cell culture plate with a density of 5×10^4 cells per well in DMEM with 10% FBS at 37 °C under 5% CO_2 for 24 h. Then, different concentrations (0, 10, 20, 40, 60, 100 μg mL^{-1} in DMEM) of **1b** were added into the plate respectively. The cells were incubated for 24 h at 37 °C under 5% CO_2. Thereafter, MTT (20 mL, 5 mg mL^{-1}) was added to each well and the plate was incubated for 4 h at 37 °C. After the addition of DMSO (100 μL per well), the cell plate was vibrated at 37 °C for 10 min. The optical density was measured at 492 nm using a microplate reader (Nanjing Huadong Electronics Group Co., Ltd. DG5033A – microplate reader).

In the bioassay assay of **1b**, the HeLa and NIH-3T3 cells were seeded into a 96-well cell culture plate with gradient density (0, 10^2, 10^3, 5×10^3, 10^4, 5×10^4, 10^5 cells per well) in DMEM with 10% FBS. After incubated 2 h at 37 °C under 5% CO_2, the cells were washed twice with PBS, 120 μL HAc–NaAc buffer solution, 50 μL of 10 mM H_2O_2 and 30 μL of 1.5 mM TMB were added in sequence. The cell plate was vibrated at 37 °C for 20 min. The optical density was measured at 653 nm using a microplate reader (Nanjing Huadong Electronics Group Co., Ltd. DG5033A – microplate reader). Different concentrations (0, 5, 10, 20, 30, 40 μg mL^{-1} in DMEM) of **1b** that incubated with certain amounts of cells (5×10^4 cells per well) were also detected.

3. Results and discussions

3.1. Nanoparticle characterization and morphology

The shape, size, and structure of the as-synthesized $CoFe_2O_4$ nanostructures have been investigated using transmission electron microscopy (TEM). Fig. 1 and S1† show representative images of four different nanostructures under different amounts of $Fe(acac)_3$ and $Co(acac)_2$. By merely changing the decomposition amount of Co and Fe precursors, the nanocrystals can be tuned in the form of near corner-grown cubic (Fig. 1A and B), near cubic (Fig. 1D and E), and nanopolyhedrons (Fig. 1G and H). Interestingly, by only changing the reaction temperature from 320 °C to 330 °C, the product shape varies from near corner-grown cubic (Fig. 1D and E) to starlike (Fig. 1J and K). All of the products have narrow size distributions (Fig. 1C, F, I and L), and the average diameters of the NPs are 24.5 ± 5.3, 45.2 ± 15.1, 13.8 ± 4.6, and 32.1 ± 4.2 nm, respectively.

Generally, the particle size mainly depends on the nuclei speed. The rapid nuclei speed obtains the small size particle, and the large particle is formed when the nuclei speed is slow.[19] When the precursor concentration is high, the nuclei speed is fast. So the size decreases with the increasing precursor concentration. But the NPs size then decreased to 25 nm at the low precursor concentration. That is largely because the nuclear concentration is too low, limiting the further growth of nanoparticles. The shape of a nanocrystal was mainly determined by the ratio of the growth rates of different crystallographic planes.[20] Several studies have reported that controlling the nucleation and growth dynamics by changing the heating rate, temperature, and the precursor concentration can result in the formation of differently shaped nanocrystals. In our

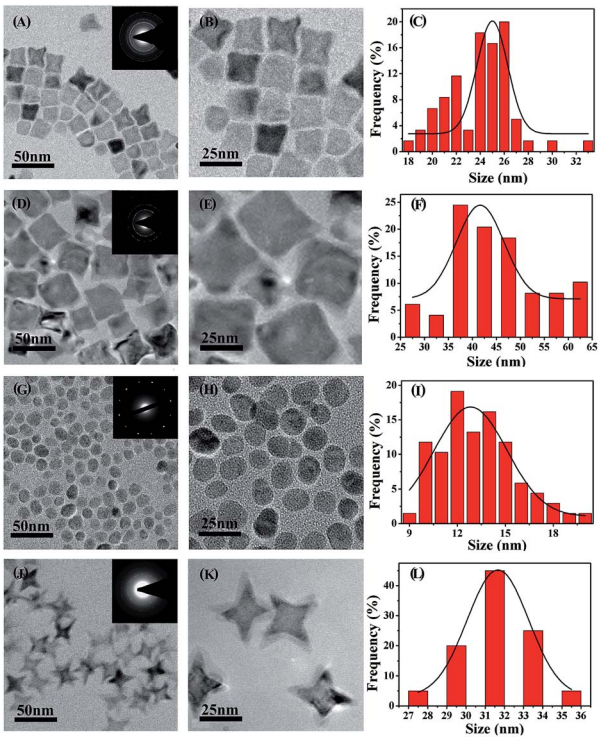

Fig. 1 TEM images of the as asythesized $CoFe_2O_4$ NPs with different shape and size. (A and B) near corner-grown cubic; (D and E) near cubic; (G and H) nanopolyhedrons; (J and K) starlike. The size distribution histograms of as-prepared $CoFe_2O_4$ NPs with the different average sizes of (C) 24.5 ± 5.3 nm, (F) 45.2 ± 15.1 nm, (I) 13.8 ± 4.6 nm, and (L) ~32.1 ± 4.2 nm.

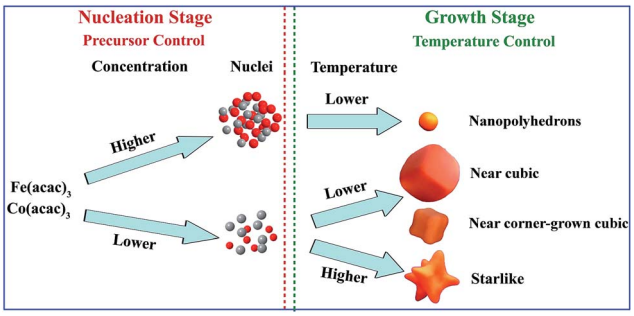

Scheme 1 Schematic illustration of the shape and size control of $CoFe_2O_4$ through adjusting the amount of precursors and heating temperature.

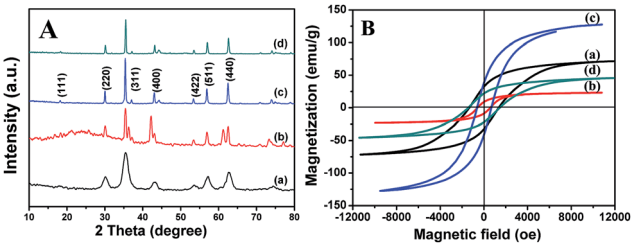

Fig. 2 (A) XRD patterns of $CoFe_2O_4$ NPs with the different average sizes (a) 13.8 ± 4.6 nm, (b) 24.5 ± 5.3 nm, (c) 32.1 ± 4.2 nm and (d) 45.2 ± 15.1 nm. (B) Magnetic hysteresis loops of (a) 13.8 ± 4.6 nm, (b) 24.5 ± 5.3 nm, (c) 32.1 ± 4.2 nm and (d) 45.2 ± 15.1 nm $CoFe_2O_4$ NPs measured at 298 K.

experiments, only oleic acid was used as the solvent and surfactant and the total volume is the same. In the low concentration of precursors, only cubic $CoFe_2O_4$ NPs are obtained. However the shapes of the obtained $CoFe_2O_4$ NPs are nanopolyhedrons in the higher concentration. These are likely because the seeds growth in the different crystal planes is sensitive to the precursor concentration. When the precursors concentration was high, the growth rates on various planes are fast that the differential growth is not significant, leading to a nanopolyhedrons shape. The gradual decrease in precursors concentration triggered the difference in the growth rate of various planes, resulting in a cubic shape. The formation of the starlike shape at 330 °C may be the continuous growth along the eight corners of the intermediate cubic shape.[21] The dependence of the shape and size on the precursor concentration and reaction temperature is shown in Scheme 1.

The crystallinity and structure of the $CoFe_2O_4$ NPs were also confirmed by powder X-ray diffraction (XRD). As shown in Fig. 2A, the peak position and relative intensity of all diffraction peaks for the four products match well with standard powder diffraction data. The half-peak width of $CoFe_2O_4$ NPs decreases with the increase of NPs sizes. The average sizes of the NPs, estimated with Scherrer's formula, are consistent with the sizes observed in the TEM images. The room-temperature hysteresis loop of the ferrites was measured using a vibrating sample magnetometer (VSM). The magnetization curves, as shown in Fig. 2B, display relatively high saturation magnetization. The saturation magnetizations (M_s) of nanopolyhedrons (13.8 ± 4.6 nm), near corner-grown cubic (24.5 ± 5.3 nm), starlike (32.1 ± 4.2 nm) and near cubic (45.2 ± 15.1 nm) were 71.7, 23.1, 127.6 and 45.7 emu g^{-1}, respectively, which indicated starlike NPs exhibited higher saturation magnetizations than near cubic and near corner-grown cubic NPs, and the nanopolyhedrons NPs exhibited medium saturation magnetizations. Generally, the moment is dependent on the NP size, and the truncated octahedral nanostructures possess lower M_s values than spherical nanostructures. The 15 nm NPs has larger particle size than that of 25 nm and 45 nm NPs, which is generally believed to be due to the presence of a magnetic dead or antiferromagnetic layer on the surface of these two NPs.[22] About this phenomenon, we will focus on the systematic investigation in future studies. The hysteresis curves of four samples suggest their ferromagnetic behavior.

The $CoFe_2O_4$ nanoparticles were also characterized by X-ray photoelectron spectroscopy (XPS). In the Co2p spectrum (Fig. 3E), the main peak at 798.2 eV with the satellite peak at 803.8 eV and that at 781.0 eV with the satellite peak at 786.9 eV belong to Co2p1/2 and Co2p3/2, respectively. The two main peaks and satellite peaks near them confirmed the presence of Co^{2+}.[23] The Fe2p spectrum in Fig. 2D exhibited one peak at ~716 eV, which is identified as the surface peak of α-Fe_2O_3.[24]

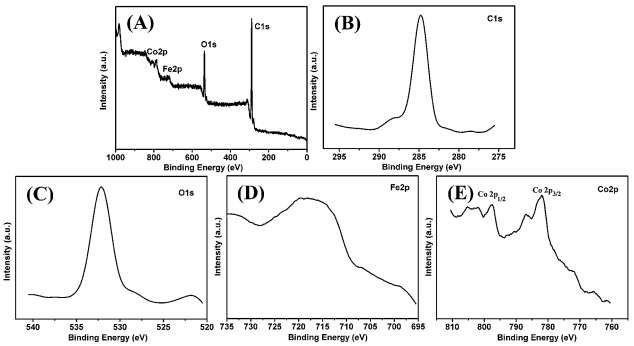

Fig. 3 (A) XPS spectra of $CoFe_2O_4$ NPs; (B) the spectrum in the C1s region; (C) the spectrum in the O1s region; (D) the spectrum in the Fe2p region; (E) the spectrum in the Co2p region.

3.2. The tunable peroxidase-like activity of the $CoFe_2O_4$ NPs

All of the monodispersed nanoparticles described above exhibited a hydrophobic surface. To modify the surface into a hydrophilic surface, the ferrite nanoparticles were treated with PEG-3,4-dihydroxy benzyl amine (DIB-PEG-NH_2). After modification with DIB-PEG-NH_2, all of the ferrite nanoparticles described above could be dispersed in water easily and the suspensions were stable (Scheme S1†).

Peroxidase-like behaviors of different water-soluble NPs (**1a**) were investigated spectrophotometrically at room temperature using 3,3′,5,5′-tetramethylbenzidine (TMB) and *o*-phenylenediamine (OPD) as the peroxidase substrate in the presence of H_2O_2. First, TMB and H_2O_2 were used to test the catalytic activity of the different **1a**. As shown in Fig. 4, all the four different shaped **1a** chosen were found to catalyze the reaction with the peroxidase substrate TMB in the presence of H_2O_2, producing a blue coloured product and exhibiting similar spectral features with their characteristic absorbance at 652 nm, except for the variations in absorbance intensity. This absorption arises from the oxidation product of TMB, similar to the phenomena observed for the commonly used horse radish peroxidase enzyme.[25] The intensity might have relevance to the catalytic activities of different **1a**. In addition, similar catalytic performance was observed when OPD was used as the substrate in place of TMB. As shown in Fig. 4A, with any of **1a**, the solutions gave an orange color with maximum absorbance at 450 nm, which originated from the oxidation product of OPD;[25] but there was still a difference in absorbance intensity for different **1a**. In contrast, it was found that **1a** or H_2O_2 alone failed to give significant color change to either TMB or OPD solution. These results indicate that all of **1a** has peroxidase-like activity toward typical peroxidase substrates in the presence of H_2O_2, but different **1a** might exhibit different catalytic activities. From the ICP, We also found that the leaching iron ions from the $CoFe_2O_4$ NPs are only 1.85%, whereas the leaching iron ions from the Fe_3O_4 NPs are 2.78%, indicating the $CoFe_2O_4$ NPs have high stability. We compared the activity of the leaching solution with that of NPs under the same conditions. As shown in Fig. S5,† the leaching solution had no activity, demonstrates

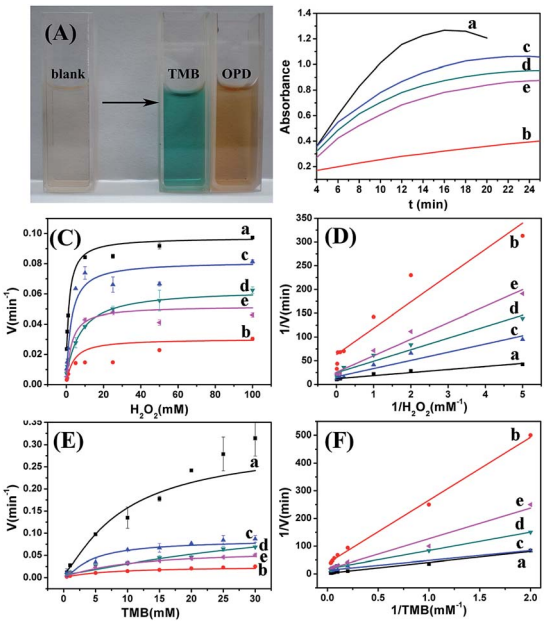

Fig. 4 (A) Photographs show production of colored product upon addition of $CoFe_2O_4$ NPs to TMB and OPD at pH 4.0. (B) The time-dependent UV absorbance curve of the HAc–NaAc solution (pH = 4.0) containing 10.0 mM H_2O_2 and 1.5 mM TMB in the presence of an equal amount of $CoFe_2O_4$ NPs for 25 min. (C) The reaction rate of different NPs in 2 mL HAc–NaAc (pH = 4.0) in the presence of 1.5 mM TMB and H_2O_2 with different concentrations at room temperature. (D) Double-reciprocal plots of activities of different NPs at a fixed concentration of TMB (1.5 mM) and varying concentrations of H_2O. (E) The reaction rate of different NPs in 2 mL HAc–NaAc (pH = 4.0) in the presence of 10 mM H_2O_2 and TMB with different concentrations at room temperature. (F) Double-reciprocal plots of activities of different NPs at a fixed concentration of H_2O_2 (10 mM) and varying concentrations of TMB. (a) 4.1 ± 0.3 nm, (b) 13.8 ± 4.6 nm, (c) 24.5 ± 5.3 nm, (d) 32.1 ± 4.2 nm and (e) 45.2 ± 15.1 nm $CoFe_2O_4$ NPs.

that the observed reaction cannot be attributed to leaching of iron ions into solution, but occurs on the surface of the NPs.

To investigate the catalytic activities of different **1a**, the substrates TMB and H_2O_2 were selected for use in a model system in the following experiments. To acquire an optimal experimental condition, the effects of pH and temperature on the catalytic activities of the **1a** were investigated. We measured the peroxidase-like activity of 4 nm, 15 nm, 25 nm, 35 nm and 45 nm **1a** while varying the pH from 2.5 to 6.0, the temperature from 20 °C to 50 °C, and the H_2O_2 concentration from 0.01 to 100 mM. From the relative catalytic activity (Fig. S2†), the optimized pH value and temperature are 4.0 and 37 °C. Therefore, we adopted pH 4.0 and 37 °C as standard conditions for subsequent analysis of **1a** activity. Likewise, the optimal H_2O_2 concentration was 10 mM (Fig. S3†). Most notably, $CoFe_2O_4$ NPs exhibited high activity over a broad pH range (2.5–6.0). As shown in Fig. S2,† the peroxidase-like activity of 4.1 ± 0.3 nm $CoFe_2O_4$ NPs could reach about 23.4% at pH 6.0 compared to that at pH 4.0.

Also, the time-dependent catalytic activities of the different **1a** were investigated under the optimized catalytic conditions. The results are given in Fig. 4B. The different **1a** showed

different levels of activity over the reaction time, in the order of spherical (4.1 ± 0.3 nm) > near corner-grown cubic (24.5 ± 5.3 nm) > starlike (32.1 ± 4.2 nm) > near cubic (45.2 ± 15.1 nm) > nanopolyhedrons (13.8 ± 4.6 nm). We also found that the catalytic activity decreases with increasing particle size under the similar morphology. Generally, the catalytic performance could be specifically regulated either by the crystal size or morphology with distinct crystallographic planes. The reason might be that different crystal sizes or planes exhibit different numbers of dangling bonds and different atom arrangement manners, which intrinsically determine the reactivity and selectivity of catalysts.[26]

In order to investigate the kinetic mechanism of the peroxidase activity of the **1a** and compare the peroxidase-like activities of the different kinds of NPs reported in this paper, apparent steady-state kinetic parameters for the peroxidase-like color reaction were determined by changing the concentration of the substrate (TMB and H_2O_2) while keeping the other concentration constant. We observed that the oxidation reaction catalyzed by the different kinds of NPs follows a Michaelis–Menten behavior towards both components, TMB and H_2O_2 (Fig. 4C and E). The Michaelis constants (K_m) were determined to explore the correlation between the structures and the activities. The K_m values of the different kinds of NPs towards different substrates were obtained and are shown in Fig. 4D and F. The K_m values of spherical, nanopolyhedrons, near corner-grown cubic, starlike and near cubic with TMB as the substrate are 0.007, 0.055, 0.017, 0.024 and 0.035 mM, respectively, and with H_2O_2 as the substrate the corresponding K_m values are 0.036, 0.228, 0.039, 0.066 and 0.111 mM, respectively (Fig. 4A). The results indicated that the spherical NPs with the size of 4 nm had the highest affinity for TMB and H_2O_2, and nanopolyhedrons NPs exhibited the lowest affinity for TMB and H_2O_2. However, the starlike NPs, near corner-grown cubic NPs, and near cubic NPs showed medium affinity. Interestingly, the apparent K_m value for the $CoFe_2O_4$ NPs (4 nm) with H_2O_2 or TMB as the substrate was lower than HRP (0.062 mM)[27] and Fe_3O_4 NPs (0.010 mM, Table S3†), suggesting that the $CoFe_2O_4$ NPs had higher affinity for H_2O_2 or TMB than HRP and Fe_3O_4 NPs which might be a reason for the enhanced peroxidase-like activity.

3.3. Mechanism of peroxidase-like activity of $CoFe_2O_4$ NPs

In general, in the magnetic MNPs catalysts for the oxidation of TMB, MNPs firstly bind and react with the H_2O_2 molecules to generate the ˙OH. Second, TMB was oxidized by ˙OH to form a blue color product.[28] To evidence mechanism of $CoFe_2O_4$ NPs catalysts for the oxidation of TMB, 50 mM H_2O_2, 0.4 mM terephthalic acid in DMF, and different concentrations (0, 5, 10, 15, 20, 25 and 30 μg) of the $CoFe_2O_4$ NPs incubating in 0.2 mM HAc–NaAc buffer (pH = 4.0) at 40 °C for 10 h.

It was clearly shown that gradual increase of the fluorescence intensity was observed as the concentration of the $CoFe_2O_4$ NPs increased, suggesting that the amount of generated ˙OH was increased by the increase in $CoFe_2O_4$ NPs. However, there was no fluorescence intensity in the absence of H_2O_2 (Fig. 5B). The

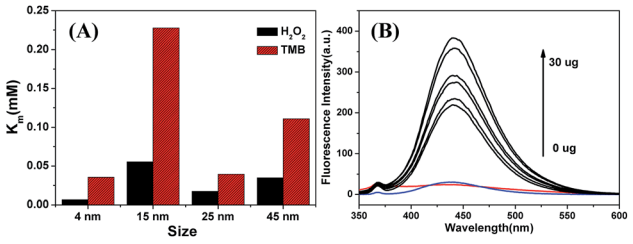

Fig. 5 (A) The Michaelis constants K_m values of the different kinds of $CoFe_2O_4$ nanoparticles towards H_2O_2 (the black bars) and TMB (the red bars). (B) Fluorescence spectral changes observed during the added of $CoFe_2O_4$ (0 μg to 30 μg) in terephthalic acid solution (excitation at 315 nm), the red line was without the H_2O_2, and the blue line was with 0 μg NPs.

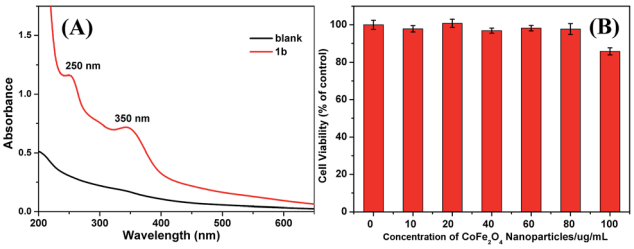

Fig. 6 (A) UV-vis detection of **1b**. The absorbance peaks at 250 nm and 350 nm belong to folic acid (FA). (B) *In vitro* cell viability of HeLa cells incubated with **1b** with different concentrations (0, 10, 20, 40, 60, 100 μg mL^{-1}).

same phenomena was also happened in $ZnFe_2O_4$ NPs–terephthalic acid–H_2O_2 system.[27] These results indicated that $CoFe_2O_4$ NPs could decompose H_2O_2 to generate the ˙OH radical, and the catalytic mechanism for the oxidation of TMB is same as the chen' report.[27]

3.4. Cytotoxicity assay of 1b

As one of the most commonly employed small molecules, folic acid (FA) could target the folate receptor present on the surface of tumor cells. Therefore, we used the FA to modify the 25 nm near corner-grown cubic $CoFe_2O_4$ NPs. The resulting **1b** was detected by UV-vis spectra to confirm that if the FA molecules were conjugated to $CoFe_2O_4$ nanoparticles. As shown in Fig. 6A, the characteristic absorption peak at around 250 nm and 350 nm appeared, respectively, which is from FA, indicating the presence of FA in **1b**. Prior to the determination of the expression of the folate receptor in cancer cells by **1b**, the cytotoxicity of the NPs was evaluated *via* an MTT assay of the viability of the HeLa cells. After the cells were incubated with different concentrations of **1b** for 24 h, no obvious decrease in cell viability was observed (Fig. 6B), which indicated that **1b** was low cytotoxicity in the given concentration range, and the **1b** was essential for further biological applications.

3.5. Targeting and detecting cancer cells

To investigate if **1b** could be used for specific detection of cancer cells (Scheme 2), HeLa cells are used, which was reported

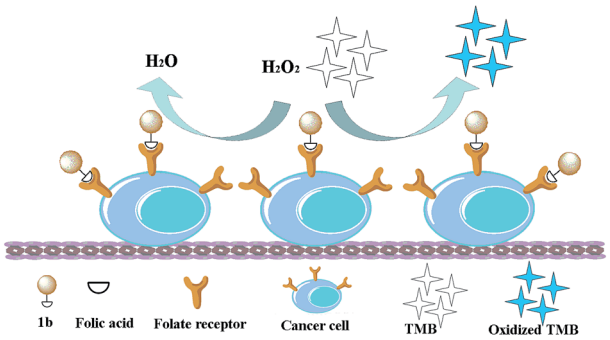

Scheme 2 Colorimetric determination of target cancer cells based on **1b**.

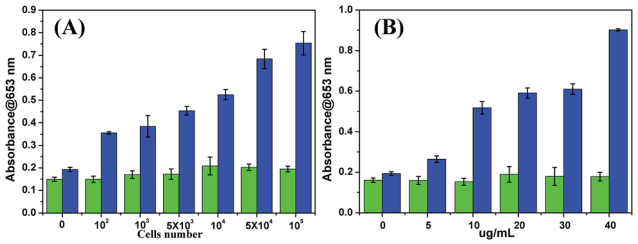

Fig. 7 Colorimetric determination of the expression of the folate receptor in cancer cells using **1b**-mediated ELISA detection of folate receptor-expressing cells. (A) The absorption values at 653 nm after 20 min depend on the number of cells. (B) The absorption values at 653 nm after 20 min with different concentrations of **1b**. TMB was used as the substrate. HeLa cells: blue bars, NIH-3T3 cells: green bars.

to overexpress folate receptor on the cell surface, and the NIH-3T3 cells has no folate receptor expression level for comparison.[29]

In our initial experiment, the 25 nm sized FA-coated $CoFe_2O_4$ NPs (**1b**) was chosen as a model study. Then both the HeLa and NIH-3T3 cells were incubated with **1b** for 2 h and subjected to monitor at 653 nm using a microtiter plate reader. As shown in Fig. 7, the absorbance of **1b** incubated with HeLa cells at 653 nm was much higher than which incubated with NIH-3T3 cells. Result shows that with the increase of HeLa cells number or the concentrations of **1b**, the absorbance gradually improved. The absorbance, however, had not been matched by increasing the number of NIH3T3 cells or the concentrations of **1b**. This clearly indicates that the proposed **1b** is suited for the simple discrimination of FA-positive cancerous cells from normal cells.

4. Conclusion

In summary, we have developed a simple precursors mediated growth method to prepare monodisperse $CoFe_2O_4$ NPs with controlled sizes and shape. Through controlled the amount of $Fe(acac)_3$ and $Co(acac)_2$, near cubic, starlike, near corner-grown cubic and nanopolyhedrons $CoFe_2O_4$ NPs with sizes of 45.2 ± 15.1, 32.1 ± 4.2, 24.5 ± 5.3 and 13.8 ± 4.6 nm, respectively, can be successfully fabricated, suggesting the amounts of iron and cobalt precursors play important roles in the manipulation of the morphology and dimensions of $CoFe_2O_4$ NPs. These $CoFe_2O_4$ NPs had different size and exposed crystal planes, and thus exhibited different levels of peroxidase-like activities, in the order of spherical (4.1 ± 0.3 nm) > near corner-grown cubic (24.5 ± 5.3 nm) > starlike (32.1 ± 4.2 nm) > near cubic (45.2 ± 15.1 nm) > nanopolyhedrons (13.8 ± 4.6 nm). This indicates that selective fabrication of peroxidase nanomimetics with different size and shape is very important to harness their catalytic activities. Based on the peroxidase-like activity, the folic acid-conjugated $CoFe_2O_4$ NPs can be used for discrimination of HeLa cells from normal breast cells. Our approach is not only useful in tuning the size, shape and catalytic performance of cobalt ferrite nanoparticles, but also offers a protocol to specifically recognize detect the cancer cells.

Acknowledgements

The work was supported by the National Natural Science Foundation of China (21271093, 81171337 and 21431002), the National Basic Research Program of China (973 Program) no. 2012CB933102, the Program for New Century Excellent Talents in University (NCET-13-0262), and the Fundamental Research Funds for the Central Universities (lzujbky-2014-k06).

Notes and references

1 (*a*) N. N. Hoover, B. J. Auten and B. D. Chandler, *J. Phys. Chem. B*, 2006, **110**, 8606; (*b*) N. Bonalumi, A. Vargas, D. Ferri, T. Bürgi, T. Mallat and A. Baiker, *J. Am. Chem. Soc.*, 2005, **127**, 8467; (*c*) S. Diezi, D. Ferri, A. Vargas, T. Mallat and A. Baiker, *J. Am. Chem. Soc.*, 2006, **128**, 4048; (*d*) C. Wang, H. Daimon, Y. Lee, J. Kim and S. H. Sun, *J. Am. Chem. Soc.*, 2007, **129**, 6974; (*e*) L. Xu, Y. Hu, C. Pelligra, C. Chen, L. Jin, H. Huang, S. Sithambaram, M. Aindow, R. Joesten and S. L. Suib, *Chem. Mater.*, 2009, **21**, 2875; (*f*) X. Wang, H. F. Wu, Q. Kuang, R. B. Huang, Z. X. Xie and L. S. Zheng, *Langmuir*, 2010, **26**, 2774; (*g*) R. Narayanan and M. A. El-sayed, *J. Am. Chem. Soc.*, 2004, **126**, 7194; (*h*) X. G. Peng, L. Manna, W. Yang, J. Wickham, E. Scher, A. Kadavanich and A. P. Alivisatos, *Nature*, 2000, **404**, 59; (*i*) H. Lee, S. E. Habas, S. Kweskin, D. Butcher, G. A. Somorjai and P. D. Yang, *Angew. Chem., Int. Ed.*, 2006, **45**, 7824; (*j*) Y. Xia, P. Yang, Y. Sun, Y. Wu, B. Mayers, B. Gates, Y. Yin, F. Kim and H. Yan, *Adv. Mater.*, 2003, **15**, 353; (*k*) Y. Yin and A. P. Alivisatos, *Nature*, 2005, **437**, 664; (*l*) P. J. Chen, S. H. Hu, C. S. Hsiao, Y. Y. Chen, D. M. Liu and S. Y. Chen, *J. Mater. Chem.*, 2011, **21**, 2535; (*m*) J. Park, J. Joo, S. G. Kwon, Y. Jang and T. Hyeon, *Angew. Chem., Int. Ed.*, 2007, **46**, 4630; (*n*) Y. Xia, Y. Xiong, B. Lim and S. E. Skrabalak, *Angew. Chem., Int. Ed.*, 2009, **48**, 60; (*o*) J. Hu, L. Li, W. Yang, L. Manna, L. Wang and A. P. Alivisatos, *Science*, 2001, **292**, 2060; (*p*) X. Wang, Q. Peng and Y. Li, *Acc. Chem. Res.*, 2007, **40**, 635.

2 (*a*) S. A. Chambers, R. F. C. Farrow, S. Maat, M. F. Toney, L. Folks, J. G. Catalano, T. P. Trainor and G. E. Brown Jr, *J. Magn. Magn. Mater.*, 2002, **246**, 124; (*b*) S. R. Naik and A. V. Salker, *J. Mater. Chem.*, 2012, **22**, 2740.

3 (*a*) A. L. C. Pereira, N. A. dos Santos, M. L. O. Ferreira, A. Albornoz and M. do C. Rangel, *Stud. Surf. Sci. Catal.*, 2007, **167**, 225; (*b*) T. Mathew, S. Shylesh, B. M. Devassy, M. Vijayaraj, C. V. V. Satyanarayana, B. S. Rao and C. S. Gopinath, *Appl. Catal., A*, 2004, **273**, 35; (*c*) M. Corrias, Y. Kihn, P. Kalck and P. Serp, *Carbon*, 2005, **43**, 2820; (*d*) M. H. Khedr, A. A. Omar and S. A. Abdel-Moaty, *Mater. Sci. Eng., A*, 2006, **432**, 26; (*e*) H. G. El-Shobaky, S. A. H. Ali and N. A. Hassan, *Mater. Sci. Eng., B*, 2007, **143**, 21.

4 M. X. Li, Y. X. Yin, C. J. Li, L. J. Zhang, S. Xu and D. G. Evans, *Chem. Commun.*, 2012, **48**, 410.

5 H. M. Joshi, Y. P. Lin, M. Aslam, P. V. Prasad, E. A. Schultz-Sikma, R. Edelman, T. Meade and V. P. Dravid, *J. Phys. Chem. C*, 2009, **113**, 17761.

6 (*a*) W. Shi, X. Zhang, S. He and Y. Huang, *Chem. Commun.*, 2011, **47**, 10785; (*b*) Y. Fan, W. Shi, X. Zhang and Y. Huang, *J. Mater. Chem. A*, 2014, **2**, 2482; (*c*) J. H. Hao, Z. Zhang, W. S. Yang, B. P. Lu, X. Ke, B. L. Zhang and J. L. Tang, *J. Mater. Chem. A*, 2013, **1**, 4352.

7 (*a*) V. Blaskov, V. Petkov, V. Rusanov, L. M. Martinez, B. Martinez, J. S. Muñoz and M. Mikhov, *J. Magn. Magn. Mater.*, 1996, **162**, 331; (*b*) F. Bensebaa, F. Zavaliche, P. L. Ecuyer, R. W. Cochrane and T. Veres, *J. Colloid Interface Sci.*, 2004, **277**, 104; (*c*) Y. I. Kim, D. Kim and S. C. Lee, *Phys. B*, 2003, **337**, 42; (*d*) R. T. Olsson, G. Salazar-Alvarez, M. S. Hedenqvist, U. W. Gedde, F. Lindberg and S. Savage, *Chem. Mater.*, 2005, **17**, 5109; (*e*) G. V. M. Jacintho, A. G. Brolo, P. Corio, P. A. Z. Suarez and J. C. Rubim, *J. Phys. Chem. C*, 2009, **113**, 7684; (*f*) T. F. O. Melo, S. W. da Silva, M. A. G. Soler, E. C. D. Lima and P. C. Morais, *Surf. Sci.*, 2006, **600**, 3642; (*g*) S. Ayyappan, G. Panneerselvam, M. P. Antony and J. Philip, *J. Mater. Chem. Phys.*, 2011, **130**, 1300.

8 (*a*) Z. P. Niu, Y. Wang and F. S. Li, *J. Mater. Sci.*, 2006, **41**, 5726; (*b*) J. C. Fu, J. L. Zhang, Y. Peng, J. G. Zhao, G. G. Tan, N. J. Mellors, E. Q. Xie and W. H. Han, *Nanoscale*, 2012, **4**, 3932.

9 (*a*) Y. Sun, G. Ji, M. Zheng, X. Chang, S. Li and Y. Zhang, *J. Mater. Chem.*, 2010, **20**, 945; (*b*) X. Wang, J. Zhuang, Q. Peng and Y. Li, *Nature*, 2005, **437**, 121; (*c*) Y. Lee, J. Lee, C. J. Bae, J. G. Park, H. J. Noh, J. H. Park and T. Hyeon, *Adv. Funct. Mater.*, 2005, **15**, 503; (*d*) K. Maaz, A. Mumtaz, S. K. Hasanain and A. Ceylan, *J. Magn. Magn. Mater.*, 2007, **308**, 289; (*e*) S. Mohapatra, S. R. Rout and A. B. Panda, *Colloids Surf., A*, 2011, **384**, 453; (*f*) S. Verma and D. Pravarthana, *Langmuir*, 2011, **27**, 13189.

10 (*a*) V. Pillai and D. O. Shah, *J. Magn. Magn. Mater.*, 1996, **163**, 243; (*b*) N. Moumen and M. P. Pileni, *Chem. Mater.*, 1996, **8**, 1128; (*c*) F. Nakagomi, S. W. da Silva, V. K. Garg, A. C. Oliveira, P. C. Morais, A. Franco Junior and E. C. D. Lima, *J. Appl. Phys.*, 2007, **101**, 09M514.

11 (*a*) M. Sorescu, A. Grabias, D. Tarabasanu-Mihaila and L. Diamandescu, *J. Appl. Phys.*, 2002, **91**, 8135; (*b*) Y. Zhang, Y. Liu, Z. Yang, R. Xiong and J. Shi, *J. Nanopart. Res.*, 2011, **13**, 4557; (*c*) S. Gyergyek, M. Drofenik and D. Makovec, *Mater. Chem. Phys.*, 2012, **133**, 515.

12 (*a*) S. Sun, C. B. Murray, D. Weller, L. Folks and A. Moser, *Science*, 2000, **287**, 1989; (*b*) C. Wang, H. Daimon, T. Onodera, T. Koda and S. Sun, *Angew. Chem., Int. Ed.*, 2008, **47**, 3588; (*c*) N. R. Jana and X. Peng, *J. Am. Chem. Soc.*, 2003, **125**, 14280; (*d*) X. Ji, X. Song, J. Li, Y. Bai, W. Yang and X. Peng, *J. Am. Chem. Soc.*, 2007, **129**, 13939; (*e*) J. Kim, S. Park, J. E. Lee, S. M. Jin, J. H. Lee, I. S. Lee, I. Yang, J. S. Kim, S. K. Kim, M. H. Cho and T. Hyeon, *Angew. Chem., Int. Ed.*, 2006, **45**, 7754; (*f*) Y. Jun, M. F. Casula, J. H. Sim, S. Y. Kim, J. Cheon and A. P. Alivisatos, *J. Am. Chem. Soc.*, 2003, **125**, 15981; (*g*) N. R. Jana, Y. Chen and X. Peng, *Chem. Mater.*, 2004, **16**, 3931; (*h*) A. Narayanaswamy, H. Xu, N. Pradhan and X. Peng, *Angew. Chem., Int. Ed.*, 2006, **45**, 5361; (*i*) J. Joo, T. Yu, Y. W. Kim, H. M. Park, F. Wu, J. Z. Zhang and T. Hyeon, *J. Am. Chem. Soc.*, 2003, **125**, 6553; (*j*) T. Yu, J. Joo, Y. Park and T. Hyeon, *Angew. Chem., Int. Ed.*, 2005, **44**, 7411; (*k*) J. Park, E. Lee, N. M. Hwang, M. Kang, S. C. Kim, Y. Hwang, J. G. Park, H. J. Noh, J. Y. Kim, J. H. Park and T. Hyeon, *Angew. Chem., Int. Ed.*, 2005, **44**, 2872; (*l*) C. Pacholski, A. Kornowski and H. Weller, *Angew. Chem., Int. Ed.*, 2002, **41**, 1188; (*m*) L. Manna, E. C. Scher and A. P. Alivisatos, *J. Am. Chem. Soc.*, 2000, **122**, 12700; (*n*) Z. A. Peng and X. Peng, *J. Am. Chem. Soc.*, 2001, **123**, 1389; (*o*) L. Manna, D. J. Milliron, A. Meisel, E. C. Scher and A. P. Alivisatos, *Nat. Mater.*, 2003, **2**, 382; (*p*) D. J. Milliron, S. M. Hughes, Y. Cui, L. Manna, J. Li, L. W. Wang and A. P. Alivisatos, *Nature*, 2004, **430**, 190; (*q*) X. Zhong, Y. Feng, W. Knoll and M. Han, *J. Am. Chem. Soc.*, 2003, **125**, 13559; (*r*) R. Si, Y. W. Zhang, L. P. You and C. H. Yan, *Angew. Chem., Int. Ed.*, 2005, **44**, 3256; (*s*) E. Lima Jr, E. L. Winkler, D. Tobia, H. E. Troiani, R. D. Zysler, E. Agostinelli and D. Fiorani, *Chem. Mater.*, 2012, **24**, 512; (*t*) S. Sun and H. Zeng, *J. Am. Chem. Soc.*, 2002, **124**, 8204.

13 (*a*) N. Bao, L. Shen, W. An, P. Padhan, C. H. Turner and A. Gupta, *Chem. Mater.*, 2009, **21**, 3458; (*b*) N. Bao, L. Shen, Y. H. A. Wang, J. Ma, D. Mazumdar and A. Gupta, *J. Am. Chem. Soc.*, 2009, **131**, 12900; (*c*) H. Zeng, P. M. Rice, S. X. Wang and S. Sun, *J. Am. Chem. Soc.*, 2004, **126**, 11458; (*d*) Q. Song and Z. J. Zhang, *J. Am. Chem. Soc.*, 2004, **126**, 6164; (*e*) J. Choi, S. J. Oh, H. Ju and J. Cheon, *Nano Lett.*, 2005, **5**, 2179; (*f*) J. Park, N. J. Kang, Y. W. Jun, S. J. Oh, H. C. Ri and J. Cheon, *ChemPhysChem*, 2002, **3**, 543.

14 (*a*) Y. Fan, W. Shi, X. Zhang and Y. Huang, *J. Mater. Chem. A*, 2014, **2**, 2482; (*b*) L. Z. Gao, J. Zhuang, L. Nie, J. B. Zhang, Y. Zhang, N. Gu, T. H. Wang, J. Feng, D. L. Yang, S. Perrett and X. Yan, *Nat. Nanotechnol.*, 2007, **2**, 577.

15 (*a*) X. Zhang, S. He, Z. Chen and Y. Huang, *J. Agric. Food Chem.*, 2013, **61**, 840; (*b*) Y. Fan and Y. Huang, *Analyst*, 2012, **137**, 1225.

16 (*a*) O. Aronov, T. Horowitz, A. Gabizon and D. Gibson, *Bioconjugate Chem.*, 2003, **14**, 563; (*b*) B. D. Wang, J. Hai, Q. Wang, T. R. Li and Z. Y. Yang, *Angew. Chem., Int. Ed.*, 2011, **5**, 3104; (*c*) Y. M. Wang, T. H. Cheng, G. C. Liu and R. S. Sheu, *J. Chem. Soc., Dalton Trans.*, 1997, **6**, 833.

17 S. H. Sun, H. Zeng, D. B. Robinson, S. Raoux, P. M. Rice, S. X. Wang and G. X. Li, *J. Am. Chem. Soc.*, 2004, **126**, 273.

18 K. Ishibashi, A. Fujishima, T. Watanabe and K. Hashimoto, *J. Photochem. Photobiol., A*, 2000, **134**, 139.
19 C. K. Taung, J. N. Kuhn, W. Huang, C. Aliaga, L. I. Hung, G. A. Somorjai and P. Yang, *J. Am. Chem. Soc.*, 2009, **131**, 5816.
20 R. H. Kodama, A. E. Berkowitz, E. J. McNiff and S. Foner, *Phys. Rev. Lett.*, 1996, **77**, 394.
21 (*a*) L. H. Hu, Q. Peng and Y. D. Li, *J. Am. Chem. Soc.*, 2008, **130**, 16136; (*b*) X. J. Zhang, C. Dong, J. Zapien, S. Ismathullakhan, Z. H. Kang, J. S. Jie, X. H. Zhang, J. Chang, C. S. Lee and S. T. Lee, *Angew. Chem.*, 2009, **121**, 9285; *Angew. Chem., Int. Ed.*, 2009, **48**, 9121; (*c*) K. B. Zhou, X. Wang, X. M. Sun, Q. Peng and Y. D. Li, *J. Catal.*, 2005, **229**, 206; (*d*) Y. Ding, F. R. Fan, Z. Q. Tian and Z. L. Wang, *Small*, 2009, **5**, 2812.
22 (*a*) B. Y. Geng, J. Z. Ma, X. W. Liu, Q. B. Du, M. G. Kong and L. D. Zhang, *Appl. Phys. Lett.*, 2007, **90**, 043120; (*b*) M. Zheng, X. C. Wu, B. S. Zou and Y. J. Wang, *J. Magn. Magn. Mater.*, 1998, **183**, 152; (*c*) Q. A. Pankhurst and R. J. Pollard, *Phys. Rev. Lett.*, 1991, **67**, 248.
23 (*a*) H. T. Zhang and X. H. Chen, *Nanotechnology*, 2005, **16**, 2288; (*b*) C. R. Brundle, T. J. Chung and D. W. Rice, *Surf. Sci.*, 1976, **60**, 286.
24 (*a*) H. Kim, D. H. Seo, H. Kim, I. Park, J. Hong, K. Y. Park and K. Kang, *Chem. Mater.*, 2012, **24**, 720; (*b*) G. K. Pradhan and K. M. Parida, *ACS Appl. Mater. Interfaces*, 2011, **3**, 317; (*c*) A. P. Grosvenor, B. A. Kobe, M. C. Biesinger and N. S. McIntyre, *Surf. Interface Anal.*, 2004, **36**, 1564; (*d*) Q. Han, Z. Liu, Y. Xu, Z. Chen, T. Wang and H. Zhang, *J. Phys. Chem. C*, 2007, **111**, 5034; (*e*) J. Lu, X. Jiao, D. Chen and W. Li, *J. Phys. Chem. C*, 2009, **113**, 4012.
25 L. Gao, J. Zhuang, L. Nie, J. Zhang, Y. Zhang, N. Gu, T. Wang, J. Feng, D. Yang, S. Perrett and X. Yan, *Nat. Nanotechnol.*, 2007, **2**, 577.
26 S. H. Liu, F. Lu, R. Xing and J. J. Zhu, *Chem.–Eur. J.*, 2011, **17**, 620.
27 L. Su, J. Feng, X. Zhou, C. Ren, H. Li and X. Chen, *Anal. Chem.*, 2012, **84**, 5753.
28 X. Sun, S. Guo, C. Chung, W. Zhu and S. Sun, *Adv. Mater.*, 2012, **25**, 132.
29 (*a*) X. Zheng, K. Kelley, H. Elnakat, W. Yan, T. Dorn and M. Ratnam, *Mol. Cell. Biol.*, 2003, **23**, 2202; (*b*) F. Bottero, A. Tomassetti, S. Canevari, S. Miotti, S. Menard and M. I. Colnaghi, *Cancer Res.*, 1993, **53**, 5791.

